

ADA042180

NSWC/DL TR-3597

12

OPTIMAL PROJECTILE SHAPES FOR MINIMUM TOTAL DRAG

by

WILLIAM W. HAGER

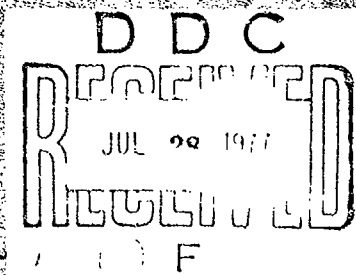
FRED B. DeJARNETTE

FRANK G. MOORE

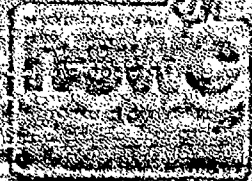
Warfare Analysis Department

MAY 1977

Approved for public release; distribution unlimited.



FILE COPY



NAVAL SURFACE WEAPONS CENTER

DAHLGREN LABORATORY
Dahlgren, Virginia 22448

WHITE OAK LABORATORY
Silver Spring, Maryland 20900

NAVAL SURFACE WEAPONS CENTER
DALLCHEN LABORATORY
Hampton, Virginia
22440

D. M. Agnew, Jr., Capt., USN
DC and Assistant Commander

UNCLASSIFIED

SECURITY CLASSIFICATION OF THIS PAGE (When Data Entered)

REPORT DOCUMENTATION PAGE		READ INSTRUCTIONS BEFORE COMPLETING FORM
1. REPORT NUMBER TR-3597	2. GOVT ACCESSION NO.	3. RECIPIENT'S CATALOG NUMBER
4. TITLE (and Subtitle) OPTIMAL PROJECTILE SHAPES FOR MINIMUM TOTAL DRAG	5. TYPE OF REPORT & PERIOD COVERED FINAL	6. PERFORMING ORG. REPORT NUMBER
7. AUTHOR(s) William W. Hager, Fred R. De Jarnette Frank G. Moore	8. CONTRACT OR GRANT NUMBER(s)	
9. PERFORMING ORGANIZATION NAME AND ADDRESS Naval Surface Weapons Center (Code DK-21) Dahlgren Laboratory Dahlgren, VA 22448	10. PROGRAM ELEMENT, PROJECT, TASK AREA & WORK UNIT NUMBERS NAVAIR TASK N00019-76-WR-61029 SEATASK 35A-501/090-1/UF32-323-505	
11. CONTROLLING OFFICE NAME AND ADDRESS Naval Air Systems Command (Code AIR-320) Washington, DC 20360	12. REPORT DATE May 1977	13. NUMBER OF PAGES 48
14. MONITORING AGENCY NAME & ADDRESS (if different from Controlling Office) Naval Sea Systems Command (Code SEA-03) Washington, DC 20360	15. SECURITY CLASS. (of this report) UNCLASSIFIED	15a. DECLASSIFICATION/DOWNGRADING SCHEDULE
16. DISTRIBUTION STATEMENT (of this Report) Approved for public release; distribution unlimited.		
17. DISTRIBUTION STATEMENT (of the abstract entered in Block 20, if different from Report)		
18. SUPPLEMENTARY NOTES		
19. KEY WORDS (Continue on reverse side if necessary and identify by block number) Optimal projectile shape Minimum drag Supersonic Mach number Newtonian theory Prandtl-Meyer expansion		
20. ABSTRACT (Continue on reverse side if necessary and identify by block number) An analytical method for theoretically predicting the projectile shape which yields the minimum total drag for a fixed length, diameter, and supersonic Mach number ($2 < M_\infty \leq 6$) is derived. The pressure drag was estimated by modified Newtonian theory on the nose and Prandtl-Meyer expansion on the afterbody. The skin friction drag was approximated by Van Driest method and the base drag by a semiempirical technique. The drag on the forebody is optimized using a new numerical technique and on the afterbody by using the method of steepest descent. The optimum body shape has a base diameter of about 70 percent of the maximum diameter and a forebody length varying between 60 and 80 percent of the total length depending on the Mach number and overall fineness ratio. The forebody ogive shape lies between the well-known hyperbolic optimum 2/3 and 3/4 power law ogives and the afterbody is conical. Results further indicate that a change of 5 percent in nose length from the optimum results in only about a 1-percent drag penalty.		

DD FORM 1 JAN 73 1473

EDITION OF 1 NOV 65 IS OBSOLETE

N 6102-101-014-6001

UNCLASSIFIED

SECURITY CLASSIFICATION OF THIS PAGE (When Data Entered)

392 59K

ACKNOWLEDGMENT

The authors would like to express their appreciation to Mr. Ralph Ferguson, a mathematician at the Naval Surface Weapons Center, White Oak Laboratory, for his assistance in the numerical calculations and to Dr. Joel Rogers of Johns Hopkins University for his contributions to the forebody optimization method.

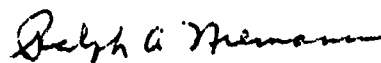
PROCESSING	
HTIS	1-17-68
DDC	1-17-68
INDEXING	1-17-68
JUSTIFICATION	1-17-68
BY	
A	

FOREWORD

This study is the first analytical attempt to optimize the total drag of Naval projectiles. The work was jointly supported by NAVAIR TASK N00019-76-WR-61029 and by SEATASK 35A-501/090-1/UF32-323-505.

This report was reviewed and approved by Mr. H. P. Caster, Head, Exterior Ballistics Division.

Released by:

A handwritten signature in cursive script, appearing to read "Ralph A. Niemann".

R. A. NIEMANN, Head
Warfare Analysis Department

TABLE OF CONTENTS

	<u>Page</u>
ACKNOWLEDGEMENT	i
FOREWORD	ii
LIST OF ILLUSTRATIONS	iv
INTRODUCTION	1
ANALYSIS	2
DRAG	2
OPTIMIZATION METHOD	8
RESULTS AND DISCUSSION	13
COMPARISON OF PRESSURE PREDICTION METHODS	13
OPTIMAL SHAPES	13
CONCLUSIONS AND RECOMMENDATIONS	20
REFERENCES	26
APPENDIX A - GLOSSARY	A-1
DISTRIBUTION	

LIST OF ILLUSTRATIONS

<u>Figure</u>	<u>Page</u>
1 Typical Body Geometry	3
2 Mean Base Pressure Coefficient	7
3 Comparison of Approximate and Exact Pressure Ratio for $M_\infty = 2$	14
4 Comparison of Approximate and Exact Pressure Ratio for $M_\infty = 3$	15
5 Comparison of Approximate and Exact Pressure Ratio for $M_\infty = 5$	16
6 Approximate Drag Coefficient as Function of Nose Length for $V/d = 4$	17
7 Approximate Drag Coefficient as Function of Nose Length for $V/d = 5$	18
8 Approximate Drag Coefficient as Function of Nose Length for $V/d = 6$	19
9 Drag Penalty for Nonoptimum Configurations for $V/d = 5$	21
10 Approximate Coefficient as Function of Nose Length for $M_\infty = 3$	22
11 Drag Penalty for Nonoptimum Configurations for $M_\infty = 3$	23
12 Optimum Body Profile for $M_\infty = 3$, $V/d = 5$ Using Approximate Theory	24
13 Drag Penalty for Having $C_f/C = 0.7$ as Function of Mach Number	25

INTRODUCTION

The external design of most projectiles was established during and prior to World War II. Few configuration changes aimed at increasing the range of these projectiles have been incorporated since that time. To achieve maximum range, the total drag, which includes pressure drag, skin friction drag, and base drag must be minimized. In 1969 one of the authors¹ developed an improved projectile shape by deriving an approximate minimum total-drag projectile based on a large amount of experimental data. Although a number of theoretical analyses has determined the shape of minimum drag bodies by considering the pressure drag and in some cases skin friction drag also, none has included the base drag as well. This report develops an analytical method for theoretically predicting the projectile shape which yields the minimum total drag for a fixed length, diameter, and supersonic Mach number ($2 \leq M_\infty \leq 6$).

A review of the literature revealed extensive research on minimum or low drag shapes, but only part of the total drag was minimized. References 2 through 10 all deal with bodies of low or minimum wave drag (pressure drag). Of particular interest is the body of minimum wave drag developed by von Karman.² The pressure distribution was estimated from slender body theory, and then the wave-drag integral was minimized by the calculus of variations. The resulting body shape is given by the relation

$$r = \frac{R}{\sqrt{\pi}} \sqrt{\phi - \frac{1}{4} \sin 2\phi}$$

where $\phi = \cos^{-1}(1 - 2x/C)$. Stivers and Spencer¹¹ calculated the total minimum-drag characteristics of four families of slender bodies at Mach numbers from 2 to 12. Of these four families, they found that the Sears-Haack profile provides the lowest total-drag coefficients at zero incidence. They did not, however, consider profiles outside these four families. Hence, there is no reason to believe that the Sears-Haack body is the optimum shape.

Cole⁶ also attempted to find a body of minimum wave drag by using the Newtonian-Busemann theory for slender bodies to estimate the pressure distribution. The body that fits these conditions is the 2/3-power law body which is described by

$$r/R = (x/C)^{2/3}$$

The von Karman body has a pointed nose whereas the 2/3-power law body has a small blunted nose. In addition to neglecting skin friction drag and base drag, both of these shapes were developed using slender body theories.

Miele⁸ attempted to optimize the body shape by minimizing the sum of the pressure drag and skin friction drag for slender bodies. As in previous cases, the body shape is simply an ogive since base drag was not considered. However, in the Mach number range at which many present and future projectiles travel ($0.7 \leq M_\infty \leq 5.0$), base drag is quite important and represents a significant portion of the total drag. In the present report, approximate yet reasonably accurate techniques are used to predict pressure, skin friction, and base drag. Then the calculus of variations is applied to determine the body shape which gives minimum total drag when the length, diameter, and Mach number are held constant.

ANALYSIS

The Mach number region of interest here will be primarily $2 \leq M_\infty \leq 6$. This covers the range of interest for projectiles with minimum time of flight requirements such as those used for antiaircraft applications. It also overlaps the Mach number range of interest for most conventional projectiles in use today, $0.5 \leq M_\infty \leq 3$. Hence, some comparison can be made between the theoretical shape derived herein with the semiempirical shape derived in Reference 1 for Mach numbers in the low supersonic regime. Also, since it has been shown that the body of minimum drag for fixed length and diameter¹ has a slightly blunted nose (bluntness ratio of $r_n/r_f \approx 0.1$), only blunt-nosed configurations will be considered.

The approach here is to use approximate analytical techniques to calculate the wave, skin friction, and base drag. Approximate techniques are necessary since the optimization procedure involves several iterations of body geometry, and use of more "exact" numerical techniques would make the computational time and storage prohibitive. On the other hand, approximate techniques will be compared with more exact methods to determine their accuracy.

DRAG

The total drag coefficient for a body of revolution at zero angle of attack is

$$C_D = \frac{2\pi}{S_f} \int_0^x C_p(x) r[r'(x)]^2 dx + C_{f_s} \frac{S_w}{S_f} - C_{p_B} \left(\frac{d_B}{d_f} \right)^2 \quad (1)$$

Referring to Figure 1, $C_p(x)$ is the pressure coefficient along the surface, C_{f_s} is the mean skin friction coefficient, and C_{p_B} is the base pressure coefficient (C_{p_B} is generally negative which makes the third term in Equation (1) positive). The first term on the right side of Equation (1) is the wave or pressure drag, the second term is the skin friction drag, and

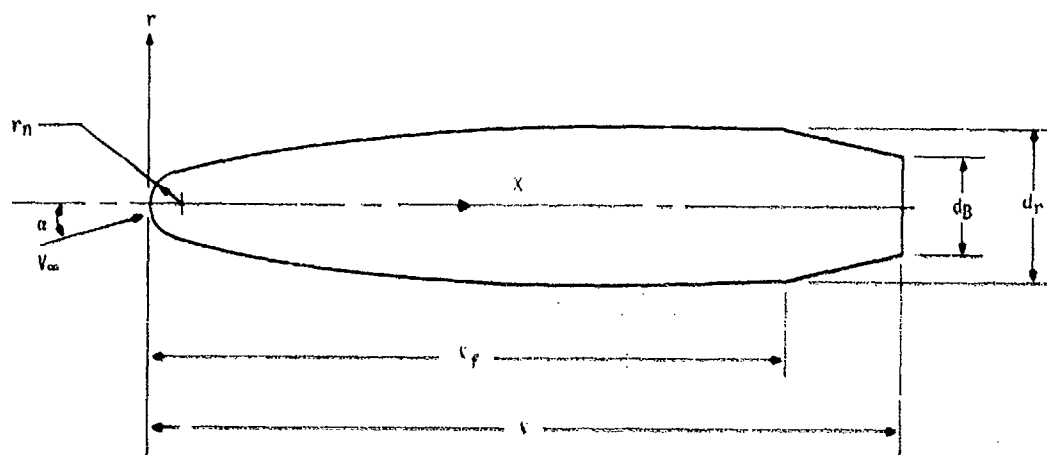


Figure 1 Typical Body Geometry

the third term is the base drag. The problem is to determine the body shape which minimizes Equation (1) subject to the constraints of fixed body length, diameter, and Mach number.

To minimize the total drag, methods are needed to predict $C_p(x)$, C_{p_n} , and C_{p_B} as functions of body shape and Mach number. These methods are discussed briefly below.

Forebody and Afterbody Pressure Coefficient

The forebody pressure coefficient is calculated from the modified Newtonian pressure distribution¹

$$C_p \approx C_{p_n} \sin^2 \theta \quad (2)$$

where θ is the body slope

$$r'(x) \approx \tan \theta \quad (3)$$

and the stagnation pressure coefficient behind a normal shock wave is

$$C_{p_0} = \frac{2}{\gamma M_\infty^2} \left\{ \left[\frac{(\gamma + 1) M_\infty^2}{2} \right]^{\frac{\gamma}{\gamma - 1}} \left[\frac{\gamma + 1}{2\gamma M_\infty^2 (\gamma - 1)} \right]^{\frac{1}{\gamma - 1}} - 1 \right\} \quad (4)$$

Equation (2) is used to calculate the pressure coefficient from the blunted nose up to the point of maximum thickness where $\theta = 0$. Although Equation (2) gives $C_p = 0$ at $\theta = 0$, which is not very accurate, the contribution of this part of the body to the overall pressure drag is small because both p and θ are small near the point of maximum thickness.

The pressure on the afterbody from the position of maximum thickness to the base is calculated from the Prandtl-Meyer expansion

$$\frac{dp}{d\theta} = \frac{\gamma p M^2}{\sqrt{M^2 - 1}} \quad (5)$$

Care must be exercised to restrict the negative slope on the afterbody to values less than about 8° ($\theta_1 < 8^\circ$) or else the flow will separate and Equation (5) will not be valid.¹²

The approximate pressure distribution given by Equations (2) and (5) will be compared with "exact" inviscid numerical results from the method of Solomon, et al.¹³

Skin Friction Drag

The boundary layer will generally be turbulent over about 90 percent of the projectile body for large caliber projectiles. Since the laminar flow region is usually less than 10 percent of the total surface area, it will be assumed the entire boundary layer is turbulent. Under this assumption the total or mean skin friction coefficient, $C_{f_{\text{tot}}}$ according to Van Driest¹⁴ may be obtained from

$$\begin{aligned} \frac{0.242}{\ln(C_{f_{\text{tot}}})^{1/2}} &= (T_\infty/T_w)^{1/2} (\sin^{-1} C_1 + \sin^{-1} C_2) \\ &= \log_{10} (R_{A_1} C_{f_{\text{tot}}}) + \left(\frac{1 + \frac{2\gamma}{\gamma - 1}}{2} \right) \log_{10} (T_\infty/T_w) \end{aligned} \quad (6)$$

where

$$C_1 = \frac{242}{(R^2 + 4.1)^{1/2}}, \quad C_2 = \frac{R}{(R^2 + 4.1)^{1/2}}$$

and

$$A = \left[\frac{(\gamma - 1) M_\infty^2}{2 T_w / T_\infty} \right]^{1/2}; \quad B = \frac{1 + (\gamma - 1) M_\infty^2}{T_w / T_\infty} - 1$$

The variable n of Equation (6) is the power in the power viscosity law

$$\frac{\mu}{\mu_\infty} = \left(\frac{T_w}{T_\infty} \right)^n \quad (7)$$

and n for air is 0.76. Equation (6) assumes a fully developed turbulent boundary layer with zero pressure gradient and Prandtl number equal to one.

In order to solve Equation (6) for the mean skin friction coefficient $C_{f,x}$, one must have values for T_w/T_∞ , R_{A_∞} , and M_∞ . The freestream Reynolds number is simply

$$R_{A_\infty} = \frac{\rho_\infty V_\infty x}{\mu_\infty} \quad (8)$$

To relate T_w/T_∞ to the freestream Mach number, assume the wall is adiabatic. Defining a turbulent recovery factor R_f by

$$R_f = \left(\frac{T_w}{T_\infty} - 1 \right) \frac{2}{(\gamma - 1) M_\infty^2}$$

then

$$\frac{T_w}{T_\infty} = 1 + R_f \frac{\gamma - 1}{2} M_\infty^2 \quad (9)$$

It is well known that the recovery factor varies as the cube root of the Prandtl number for turbulent flow so that

$$R_f = \sqrt[3]{P_r} \quad (10)$$

Recall that Van Driest's method assumes a Prandtl number of unity. If this value were used, then R_f would also be unity. However, the actual value of $P_r \approx 0.73$ so that the previous assumption of Prandtl number one can be compensated for somewhat by the above recovery factor which for $P_r = 0.73$ would be 0.90. Thus Equation (9) becomes

$$T_w/T_\infty = 1 + 0.9 \frac{\gamma - 1}{2} M_\infty^2 \quad (11)$$

Then, for a given set of freestream conditions (M_∞ , ρ_∞ , μ_∞ , V_∞) one can combine Equations (8) and (11) with (6) to solve for C_{f_∞} . The equation must be solved numerically however, since C_{f_∞} cannot be solved for explicitly. A procedure adaptable to equations of this type is the well-known Newton-Raphson method.

Once the mean skin friction coefficient has been determined for a given set of freestream conditions, the viscous drag coefficient is simply

$$C_{D_f} = C_{f_\infty} \frac{S_w}{S_r} \quad (12)$$

The wetted area, S_w , is the total surface area of the body (excluding the base) which can be integrated numerically given a set of body coordinates.

Base Drag

Much theoretical work has been performed to predict base pressure.¹² There is still no satisfactory theory available, however, and the standard practice has been to use empirical methods. This is the approach taken here. Figure 2 is a mean curve of experimental data taken from Reference 12. This data assumes a long cylindrical afterbody with a fully developed turbulent boundary layer ahead of the base. There could be deviations from this curve due to low body fineness ratio, boattails, angle of attack, Reynolds number, and surface temperature. Each of these effects are discussed in Reference 12.

The base pressure is significantly altered by the presence of a boattail so that this change must be accounted for. Probably the most simple method to do this is an empirical equation given by Stoney.¹²

$$C_{p_B} = C_{p_{B,A}} \frac{d_B}{d_r}$$

and thus

$$C_{D_B} = -C_{p_B} \left(\frac{d_B}{d_r} \right)^2 = -C_{p_{B,A}} \left(\frac{d_B}{d_r} \right)^3 \quad (13)$$

Equation (13) can be used throughout the entire Mach number range where $C_{p_{B,A}}$ is the base pressure given by the curve of Figure 2.

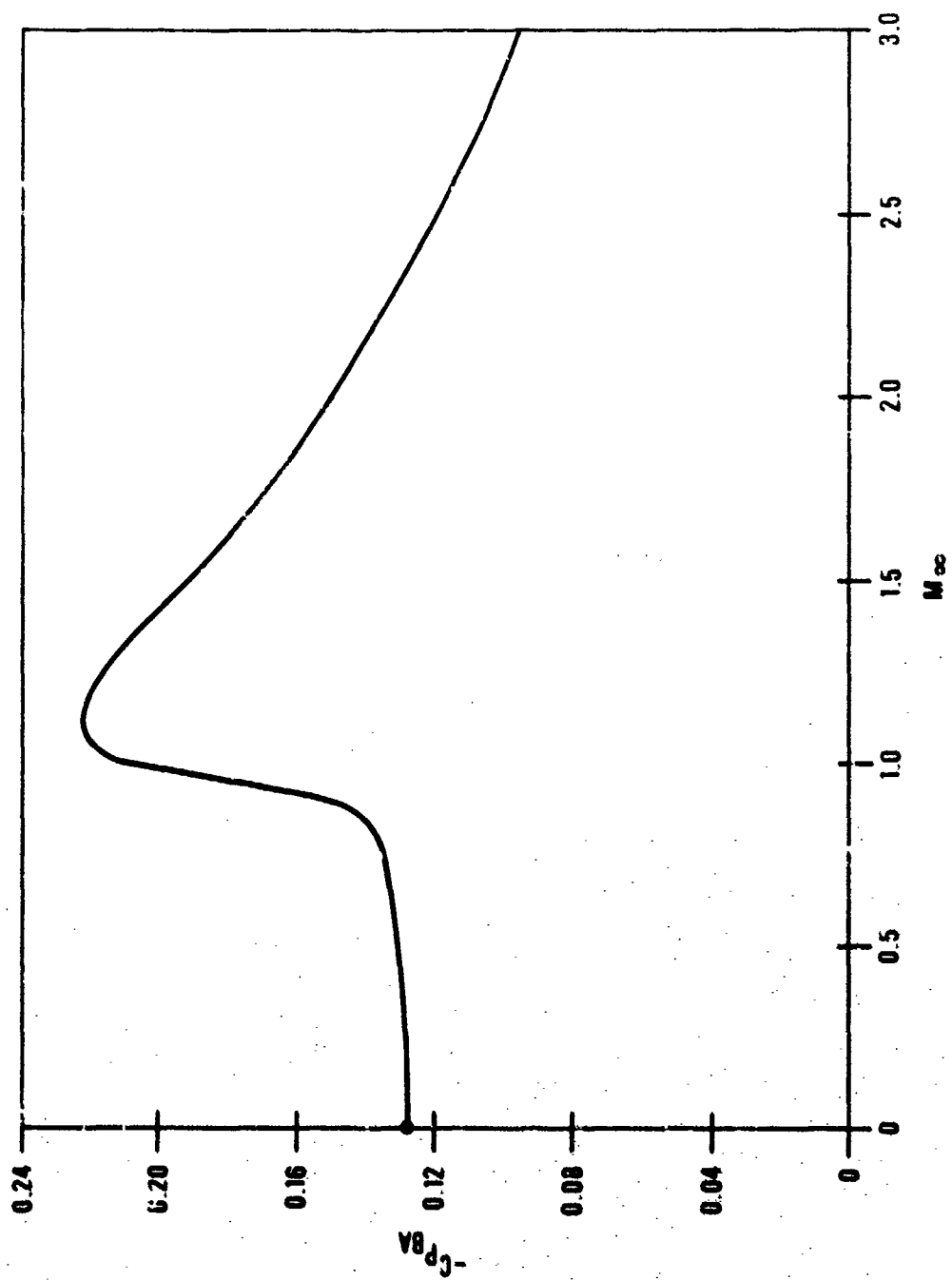


Figure 2. Mean Base Pressure Coefficient

OPTIMIZATION METHOD

The optimal shape for a fixed length, diameter, and Mach number is determined by computing the minimum-drag body for a sequence of values of the forebody length ℓ_f (refer to Figure 1). Then, the body shape corresponding to the value of ℓ_f which gives minimum total drag is the optimal shape. Hence, two distinct optimization problems must be considered: the forebody and the afterbody problems.

Forebody

A very efficient method is described below for computing the optimal forebody shape. The algorithm is based on Lagrange duality theory for convex control problems developed by Hager and Mitler.¹⁶ By solving an initial value problem, the optimal dual multiplier is computed. The optimal shape is determined using a minimum principle.

A common procedure for solving constrained variational problems is the following: An iterative method is used to approximate the solution(s) of the Euler inequality associated with the variational problem. Typical algorithms involve Newton's method or a shooting method to solve a two-point boundary value problem. These methods, however, are subject to numerical instabilities and the initial iteration must be chosen close to the optimal shape for convergence.

The present algorithm is far better than the iterative approaches since it is essentially direct—no iterations or initial guesses are involved and the scheme is completely stable. The computational procedure is described below.

The forebody optimization problem is

$$\begin{aligned} &\text{minimize} && \int_0^{\ell_f} \left[C_{f_1} r(x) \sqrt{1 + r'(x)^2} + \frac{C_{f_0} r(x) r'(x)^3}{1 + r'(x)^2} \right] dx \\ &\text{subject to} && r(0) = 0, \quad r(\ell_f) = R \end{aligned} \quad (15)$$

$$r'(x) \geq 0 \quad \text{for all } x \in [0, \ell_f]$$

where R and ℓ_f are the given radius and length of the forebody. The constraint $r'(x) \geq 0$ is imposed since $r(x)$ is nondecreasing on the forebody. Although we constrain $r(0) = 0$, a blunt nose shape can be achieved as the limit of a sequence of shapes satisfying $r(0) = 0$. The blunt nose shape could also be treated by adding an additional drag term to the extremand above that corresponds to the radius of the nose and removing the constraint $r(0) = 0$; however the analysis is easier using the formulation of Equation (15) above.

Make a change of variables and express the variational problem in terms of the independent variable, $\rho = r^2$, and the dependent variable, $g(\rho) = 1/r'$. Omitting the algebra, Equation (15) is equivalent to

$$\text{minimize} \quad \int_0^{R^2} \left[C_{f_\infty} \sqrt{g(\rho)^2 + 1} + \frac{C_{p_0}}{g(\rho)^2 + 1} \right] d\rho \quad (16)$$

$$\begin{aligned} \text{subject to} \quad & \int_0^{R^2} \frac{g(\rho)}{\sqrt{\rho}} d\rho = 2\psi_f \\ & g(\rho) \geq 0 \quad \text{for } \rho \geq 0 \end{aligned}$$

If $g(\rho)$ solves Equation (16), then the corresponding shape $r(x)$ is found by integrating the following initial value problem

$$\begin{aligned} r'(x) &= 1/g(r(x)^2) \\ r(0) &= r_n \end{aligned} \quad (17)$$

where r_n is the radius of bluntness for the nose.

As shown in Reference 16, two different types of forebody shapes can occur depending on the ratios C_{p_0}/C_{f_∞} and ψ_f/d_f . The optimal shape consists of a blunt nose followed by a smooth monotone profile whenever

$$\sqrt{(2C_{p_0}/C_{f_\infty})^{2/3} - 1} \geq \psi_f/R \quad (18)$$

If this inequality is violated, the optimal shape consists of a spike followed by a cone with slope given by

$$r'(x) = \left(\sqrt{(2C_{p_0}/C_{f_\infty})^{2/3} - 1} \right)^{1/2}$$

For realistic flight conditions, the skin friction coefficient, C_{f_∞} , is much smaller than the stagnation pressure coefficient, C_{p_0} ; hence inequality (18) is satisfied and the nose is blunt.

The algorithm for computing the blunt nose solution of Equation (16) is now described. Define the following functions

$$h(g) = C_{f_\infty} \sqrt{1+g^2} + \frac{C_{p_0}}{1+g^2} \quad (19)$$

and

$$H(g, z) = h(g) + \frac{g}{z} \quad (20)$$

The function, H , is related to the integrand of the Lagrangian of Equation (16) given by

$$\int_0^{R^2} \left[h(g(\rho)) + \frac{\lambda g(\rho)}{\sqrt{\rho}} \right] d\rho = \int_0^{R^2} H\left(g(\rho), \frac{\sqrt{\rho}}{\lambda}\right) d\rho$$

By the minimum principle,¹⁶ if $g^*(\rho)$ is an optimal solution to Equation (16), there exists a scalar λ such that

$$H(g^*(\rho), \sqrt{\rho}/\lambda) = \min\{H(g, \sqrt{\rho}/\lambda); g \geq 0\}$$

for almost every $0 \leq \rho \leq R^2$. Hence, after computing the optimal dual multiplier λ , $g^*(\rho)$ is the value of $g \geq 0$ that minimizes $H(g, \sqrt{\rho}/\lambda)$.

Let $G(z)$ be the value of $g \geq 0$ that minimizes $H(g, z)$. Analyzing the structure of the function $h(g)$, it can be shown that there exists a critical value, $z = z_0$, such that $G(z) = 0$ for $z \leq z_0$ and $G(z) > 0$ for $z > z_0$; this critical value is given by

$$z_0 = (h'(\sqrt{\alpha^2 - 1}))^{-1} \quad (21)$$

where α is the unique positive root of the equation

$$(C_{p_0} + C_{f_\infty})\alpha^3 + C_{p_0}(\alpha^2 - 2\alpha - 2) = 0 \quad (22)$$

Also, it can be shown that the slope of the nose at $x = 0$ is $1/\sqrt{\alpha^2 - 1}$ and the slope approaches 45° as $C_{f_\infty}/C_{p_0} \rightarrow 0$.

Let w_1 and w_2 satisfy the differential equations

$$\begin{aligned} w_1'(z) &= G(z) & w_2'(z) &= 2C_f/d_f \\ w_1(z_0) &= 0 & w_2(z_0) &= 2(z_0 C_f)/d_f \end{aligned} \quad (23)$$

Notice that $w_1(z_0) \leq w_2(z_0)$ and as $z \rightarrow \infty$, $G(z)$ approaches the left side of inequality (18).

Thus by inequality (18), $w'_1(z) > w'_2(z)$ for z sufficiently large, there exists \hat{z} such that $w_1(\hat{z}) = w_2(\hat{z})$. It can be shown that the optimal dual multiplier is $\lambda = r_1/\hat{z}$ and the nose bluntness is $r_n = \lambda z_0$. Hence, the solution to Equation (16) is $g^*(r) = G(r/\lambda)$, and the optimal shape $r^*(x)$ is given by Equation (17).

Afterbody

In addition to pressure drag and skin friction drag, the afterbody also has base drag. Equation (5) must be integrated to obtain the pressure drag, and the base drag is given by Equation (13). The afterbody drag coefficient to be minimized thus becomes

$$C_{D,AB} = \frac{8}{d_f^2} \int_{x_f}^x \left\{ \frac{2}{\gamma M_\infty^2} \left(\frac{p}{p_\infty} - 1 \right) r(x) q(x) + C_{f,\infty} r(x) \sqrt{1+q^2} \right\} dx + \frac{C_{p,BA} r(x)^3}{8d_f^3} \quad (24)$$

subject to

$$r'(x) = q(x)$$

$$q'(x) = u(x)$$

$$p'(x) = \frac{\gamma u(x)}{1+q^2} \frac{p(x) M(p)^2}{\sqrt{M^2-1}}$$

(25)

The initial conditions are at the beginning of the afterbody where

$$r(x_f) = d_f/2 \quad (26)$$

$$q(x_f) = 0 \quad (27)$$

$$p(x_f) = p_\infty \quad (28)$$

The variable $u(x) = q'(x) = r''(x)$ is to be chosen to minimize the drag coefficient. Equation (27) implies the body slope at the beginning of the afterbody is zero. Now the slope at the end of the forebody is generally nonzero, therefore, there can be a slope discontinuity at $x = x_f$. Equation (28) gives the beginning pressure as p_∞ ($C_{p_f} \approx 0$) which is consistent with modified Newtonian theory. The Mach number on the surface is related to the surface pressure by the isentropic relation

$$M(p)^2 = \frac{2}{\gamma-1} \left[\left(\frac{p_n}{p} \right)^{\frac{\gamma-1}{\gamma}} - 1 \right] \quad (29)$$

where the stagnation pressure is given by

$$p_0 = p_\infty \left[\frac{\gamma}{2} M_\infty^2 C_{p_0} + 1 \right] \quad (30)$$

In Equation (25) the independent variable for $p'(x)$ was changed from θ in Equation (5) to x by use of the geometric relation

$$\frac{d\theta}{dx} = \frac{u(x)}{1 + q(x)^2} \quad (31)$$

As used in control theory terminology, the function u above is the control variable and the functions r , q , and p are the state variables.

The Euler approximation is used to replace the integral and derivatives in Equation (24) by the following discretization

$$\text{minimize} \quad \left\{ C_{p_{N+1}} \left(\frac{2v_1^N}{d_r} \right)^2 + \sum_{n=0}^{N-1} L(x^n) \Delta x \right\} \quad (32)$$

$$\text{subject to} \quad \left. \begin{aligned} x^{n+1} &= x^n + \Delta x F(x^n, u^n) \\ x^n &= \begin{bmatrix} x_1^n \\ x_2^n \\ x_3^n \end{bmatrix} = \begin{bmatrix} r^n \\ q^n \\ p^n \end{bmatrix} \\ x_1^0 &= d_r / \Delta, \quad x_2^0 = 0, \quad x_3^0 = p_\infty \end{aligned} \right\} \quad (33)$$

where $[r^n, q^n, p^n]$ are approximations to $[r(x_n), q(x_n), p(x_n)]$, $L(r, q, p)$ denotes the integrand in Equation (24), and the vector function $F(r, q, p, u)$ denotes the right side of the differential equations in Equation (25).

The solution to Equation (32) was computed by the method of steepest descent. Define

$$H(x^n, u^n, \lambda^n) = L(x^n) + F(x^n, u^n)^T \lambda^n \quad (34)$$

and let $\{\lambda^n\}$ denote the sequence of dual multiplier vectors given by

$$\lambda^{n+1} = \lambda^n + \Delta x \frac{\partial}{\partial u^n} H(x^n(u^n), u^n, \lambda^n) \quad (35)$$

where $y^n(u^n)$ is the solution of the difference Equation (32) for given $\{u^n\}$. Starting with an initial guess to the optimal control, the control is incremented by the rule

$$u_{(new)}^n = u_{(old)}^n - \epsilon \Delta x \frac{\partial}{\partial u^n} [H(y^n, u^n, \lambda^n)]_{(old)} \quad (36)$$

For the argument of H in Equation (36), y^n is determined by the difference Equation (32) and λ^n is determined by Equation (35) for given $u_{(old)}^n$. The parameter $\epsilon > 0$ is chosen small enough to reduce the drag for the new discrete control approximation. For the bodies studied in this report, $\epsilon \approx 40$ gave the most rapid convergence in the discrete control.

RESULTS AND DISCUSSION

COMPARISON OF PRESSURE PREDICTION METHODS

To test the accuracy of the methods used to calculate the pressure drag, Equations (2) and (5) are compared with numerical results from the method of Solomon, et al.¹³ Figures 3, 4, and 5 compare the pressure distributions over the original nose-boattail body given by the equation

$$r = [15 + 2v - v^2]^{1/2} / \sqrt{15}, \quad 0 \leq v \leq 1.75 \quad (37)$$

for $M_\infty = 2, 3$, and 5 , respectively. The forebody pressure was computed by two methods: (a) Equation (2), and (b) the modified Newtonian-Busemann pressure distribution which includes the curvature effect.⁸ These three figures show that Equation (2) predicts the forebody pressure reasonably well, and Equation (5) gives pressures reasonably close to the "exact" solution on the afterbody. Actually the calculated drag is quite good because the pressure is too high near the maximum thickness and too low near the base. These two effects introduce partially compensating errors. In all three figures, the curvature effect drives the pressure too low, hence, this method was not used in the optimization process.

OPTIMAL SHAPES

For fixed values of C/d and M_∞ , minimum drag body shapes were calculated for forebody lengths of $C_f/C = 0.5, 0.6, 0.7, 0.8$, and 0.9 . Then the optimum value of C_f/C (for a given C/d and M_∞) is the value corresponding to the minimum C_D . Figures 6, 7, and 8 show the effect of C_f/C on C_D for C/d values of $4, 5$, and 6 , respectively. Each figure

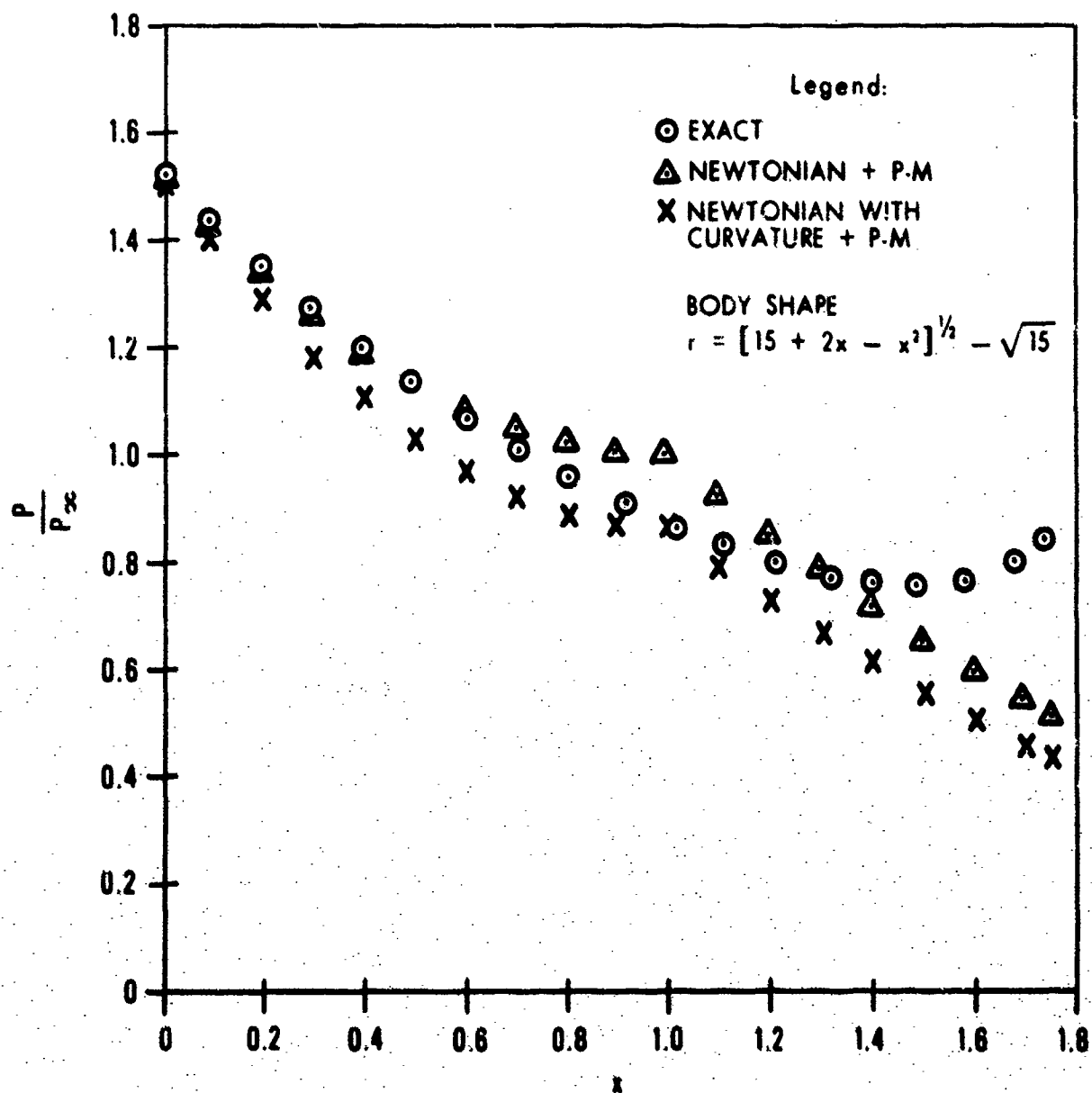


Figure 1. Comparison of Approximate and Exact Pressure Ratio for $M_\infty = 2$.

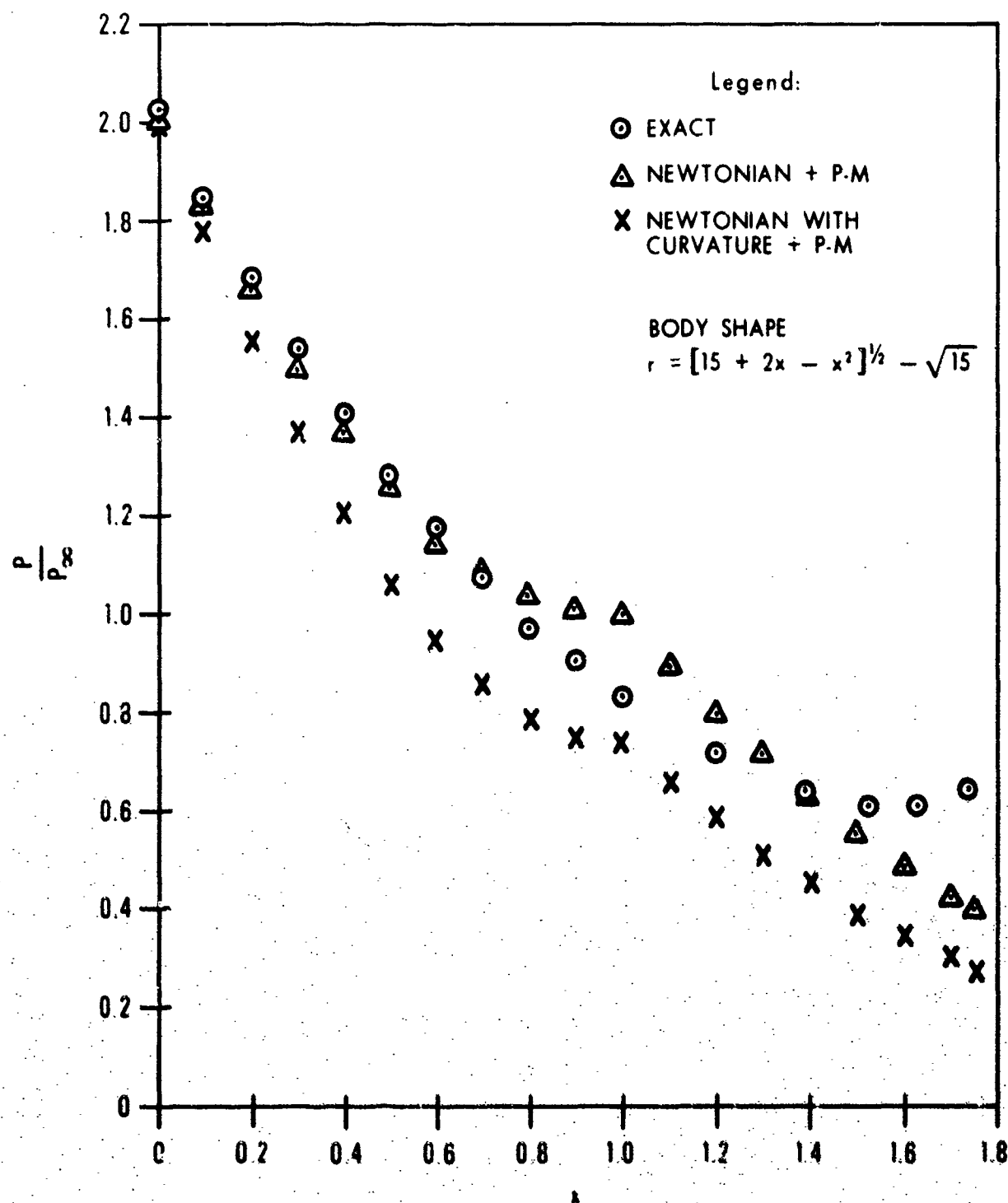


Figure 4 Comparison of Approximate and Exact Pressure Ratio for $M_\infty = 1$

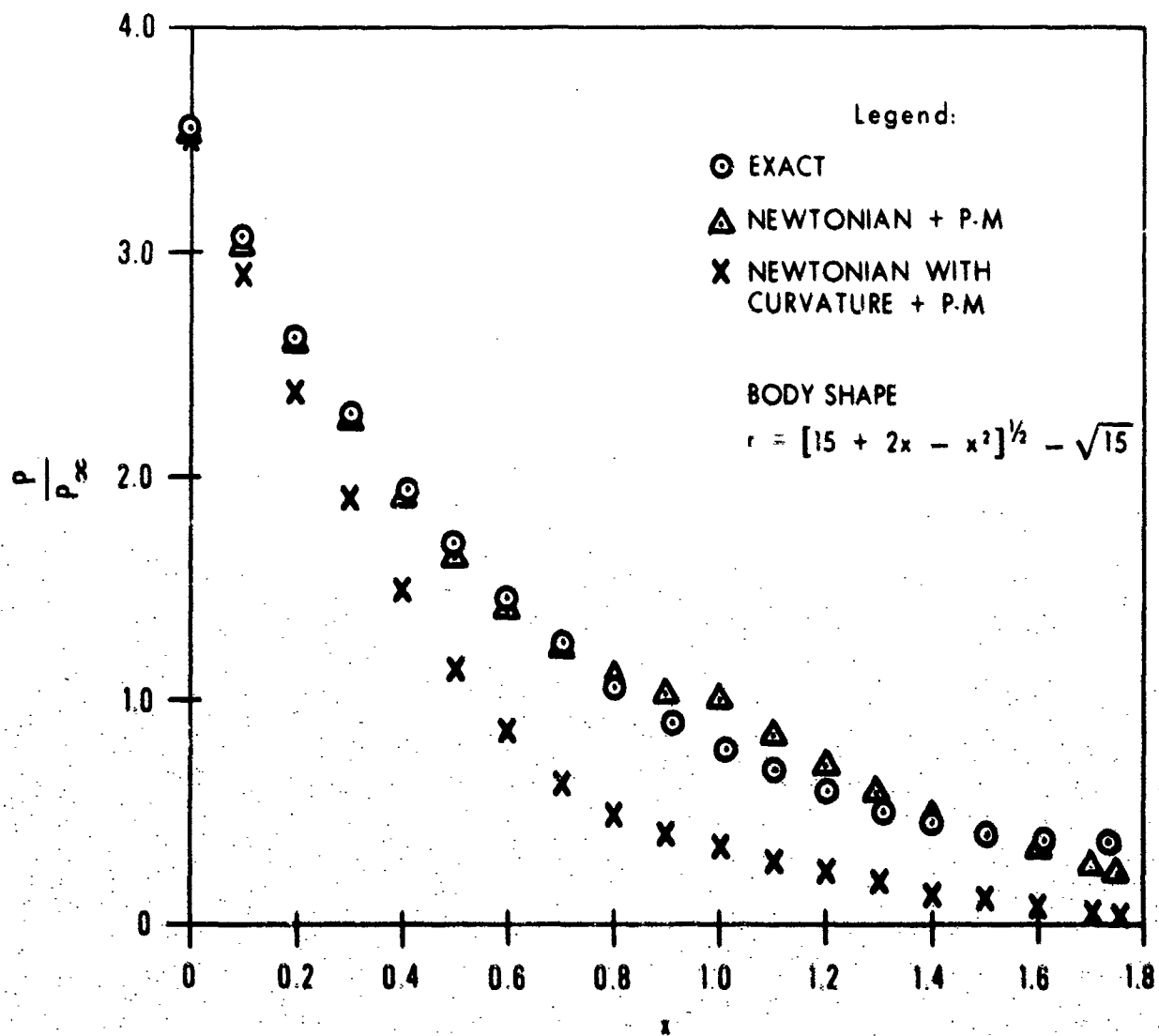


Figure 4. Comparison of Approximate Exact Pressure Ratios for $M_\infty = 5$

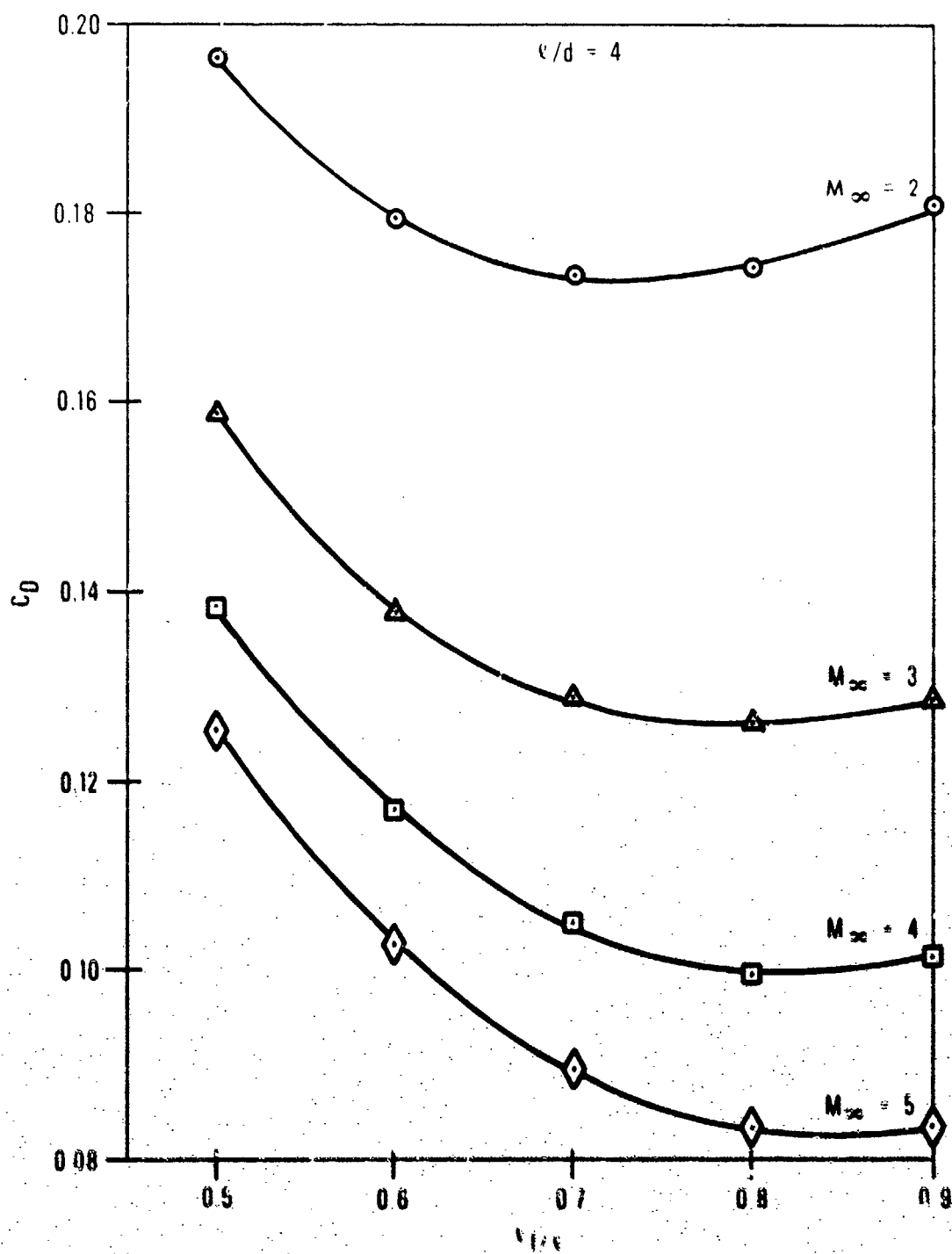


Figure 6. Approximate Drag Coefficient as Function of Nose Length for $c/d = 4$

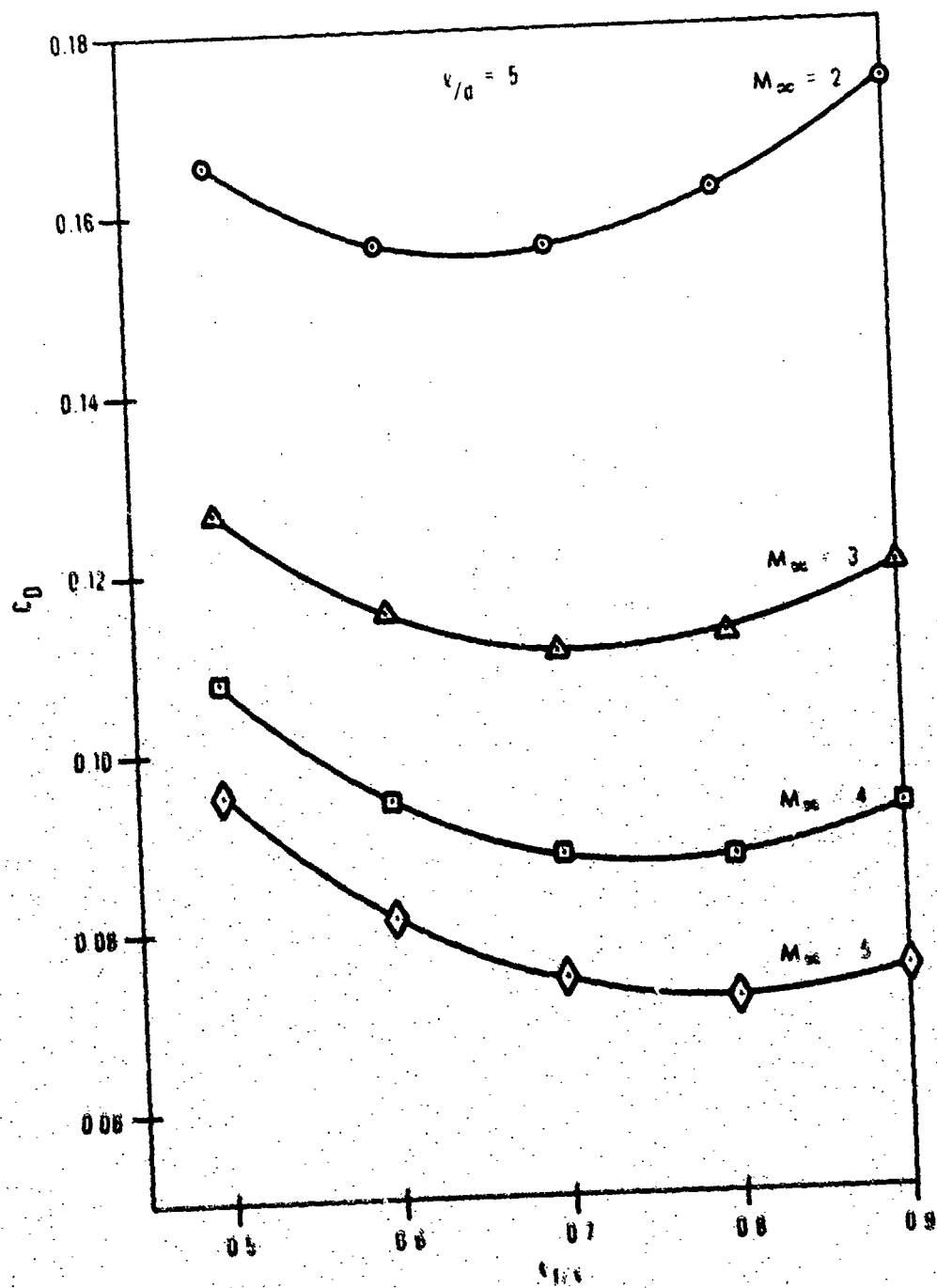


Figure 7 Approximate Drag Coefficient as Function of Nose Length for $y/d = 5$

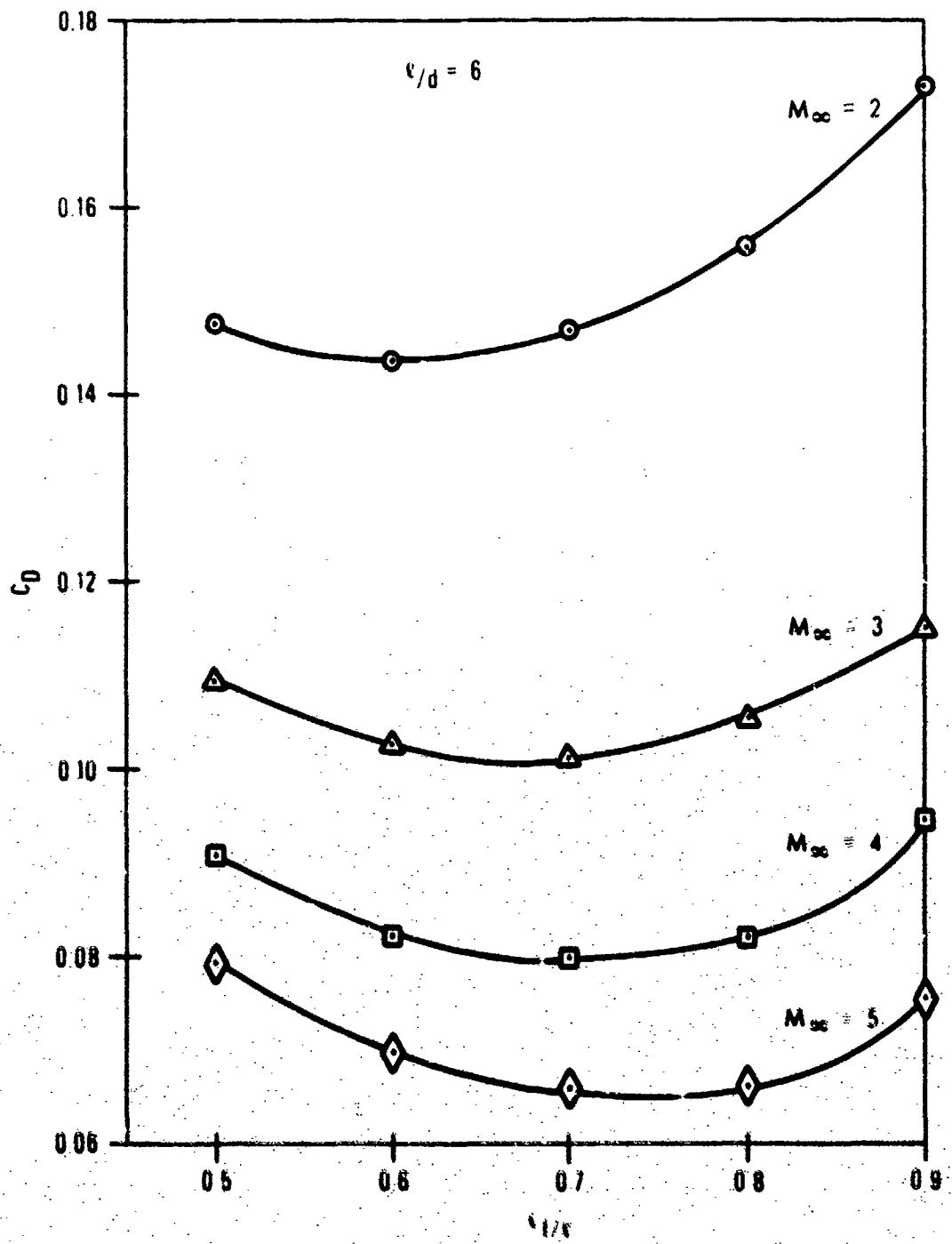


Figure 8. Approximate Drag Coefficient as function of Tip Length for $b/d = 6$.

gives the results for $M_\infty = 2, 3, 4$ and 5 . Note that each curve indicates that the value of ℓ_f/ℓ corresponding to minimum C_D is not sharply defined. In fact, Figure 9 shows that for $\ell/d = 5$, ℓ_f/ℓ which gives minimum C_D varies almost linearly with M_∞ , and that $\Delta\ell_f/\ell \approx \pm 0.05$ only increases the minimum C_D by about 1 percent. Also, Figure 10 illustrates the effect of ℓ_f/ℓ on C_D for $M_\infty = 3$ and $\ell/d = 4, 5, 6$, and 7 . A cross plot of this figure is shown in Figure 11 which depicts the optimal ℓ_f/ℓ as varying almost linearly with ℓ/d and a range of $\Delta\ell_f/\ell \approx \pm 0.05$ only increases $C_{D_{min}}$ by about 1 percent.

The optimal shape for $M_\infty = 3$ and $\ell/d = 5$ is illustrated in Figure 12. This shape is close to that found by Moore¹ using semiempirical techniques. The forebody has a value of $\ell_f/\ell = 0.7$ and the base diameter ratio is $d_B/d_f = 0.7$. From considerations of the internal ballistics of projectiles, the value of ℓ_f/ℓ is limited to about 0.65 to 0.7 unless forward-mounted sabots are used for launching the projectile. However, as shown in Figures 9 and 11, even though the point of maximum diameter may not be at the optimum location, only a small drag penalty is paid for a ± 5 -percent variation in ℓ_f/ℓ from the optimum.

Figure 13 shows the variation of C_D with M_∞ for $\ell/d = 4, 5$, and 6 . The curve designated $C_{D_{min}}$ is the drag coefficient for the optimal shape at each M_∞ and ℓ/d . Hence the value for ℓ_f/ℓ is different for each M_∞ and ℓ/d . The dashed curves give the variation of C_D with M_∞ for a fixed value of $\ell_f/\ell = 0.7$. This figure illustrates that $\ell_f/\ell = 0.7$ gives nearly minimum drag for $\ell/d = 5$ and 6 over the range $2 \leq M_\infty \leq 5$.

CONCLUSIONS AND RECOMMENDATIONS

1. A numerical method has been developed for calculating the optimal projectile shape which produces minimum total drag.
2. The optimal shape changes with ℓ/d and Mach number. For $\ell/d = 5$ a nose length of $\ell_f/\ell = 0.7$ gives nearly the optimum shape over the range of $2 \leq M_\infty \leq 5$.
3. A variation in nose length of $\Delta\ell_f/\ell \approx \pm 0.05$ results in only about a 1-percent increase in total drag.
4. The optimum shapes have a base diameter of about 0.7 times the maximum diameter.
5. It is recommended that a similar optimization be performed for subsonic and transonic Mach numbers.
6. While it is believed the optimum body shape derived from the approximate theory is reasonably accurate, should an exact theory be used for the pressure prediction instead of the approximate theory, the absolute value of the drag coefficient may be in substantial error, particularly at the low supersonic Mach numbers. For this reason, it is believed the expenditure involved in using an exact theory such as that of Solomon¹³ to repeat the present work is justified. This effort will be started in FY 77 at NSWC/DL.

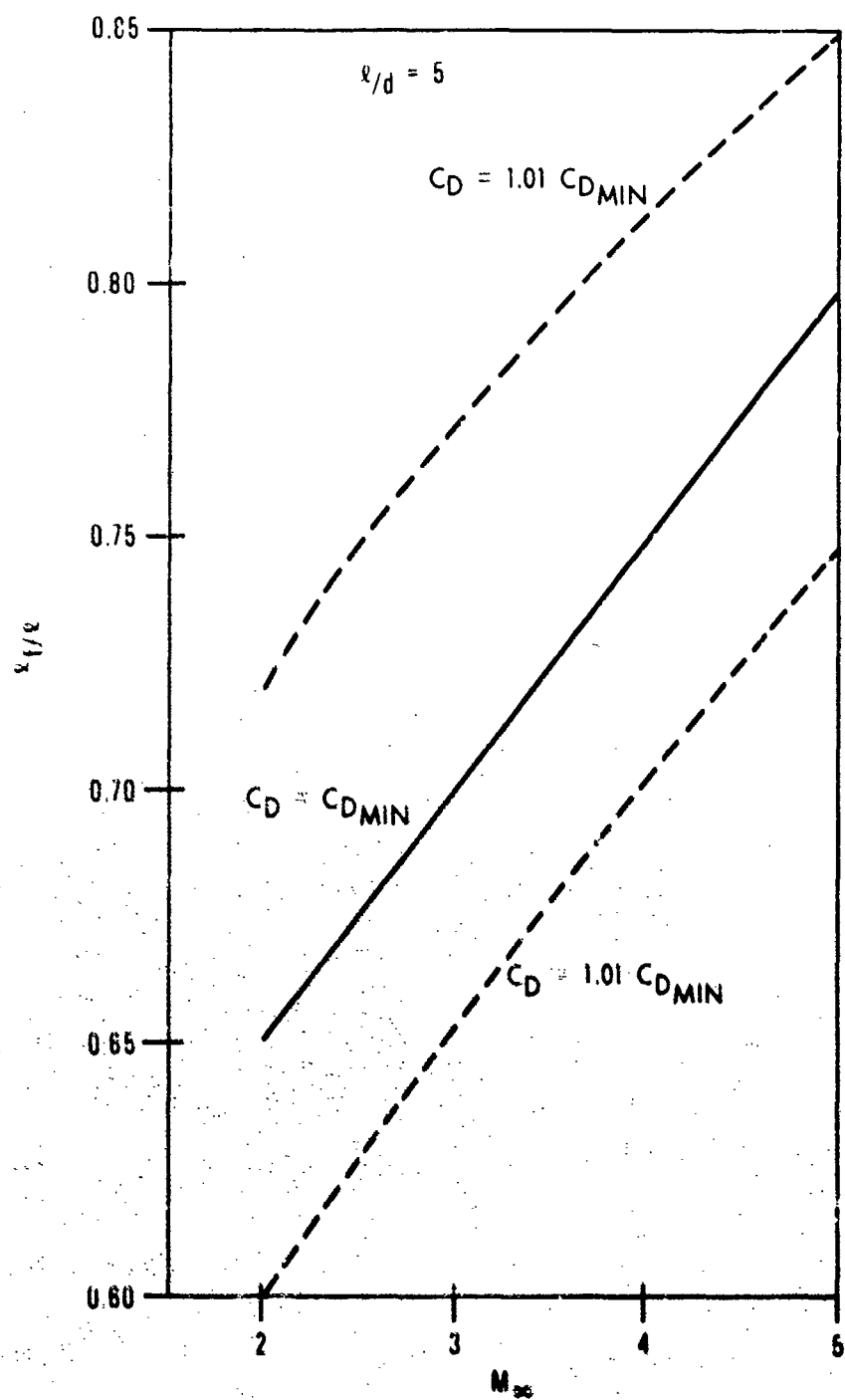


Figure 9 : Drag Penalty for Nonoptimum Configurations for $l/d = 5$

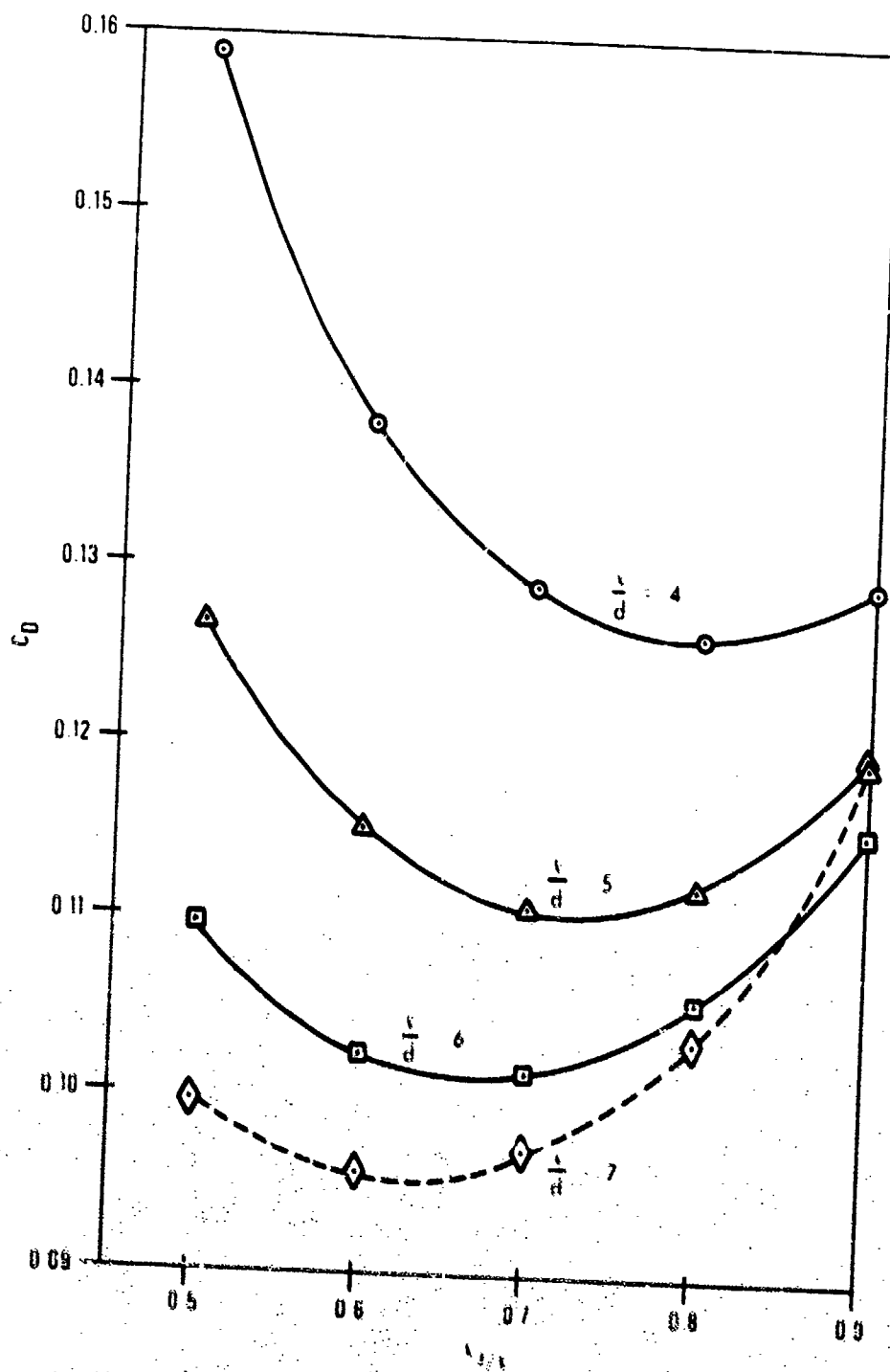


Figure 10. Approximate Drag Coefficient as Function of Nose Length for $M_\infty = 4, 5, 6, 7$.

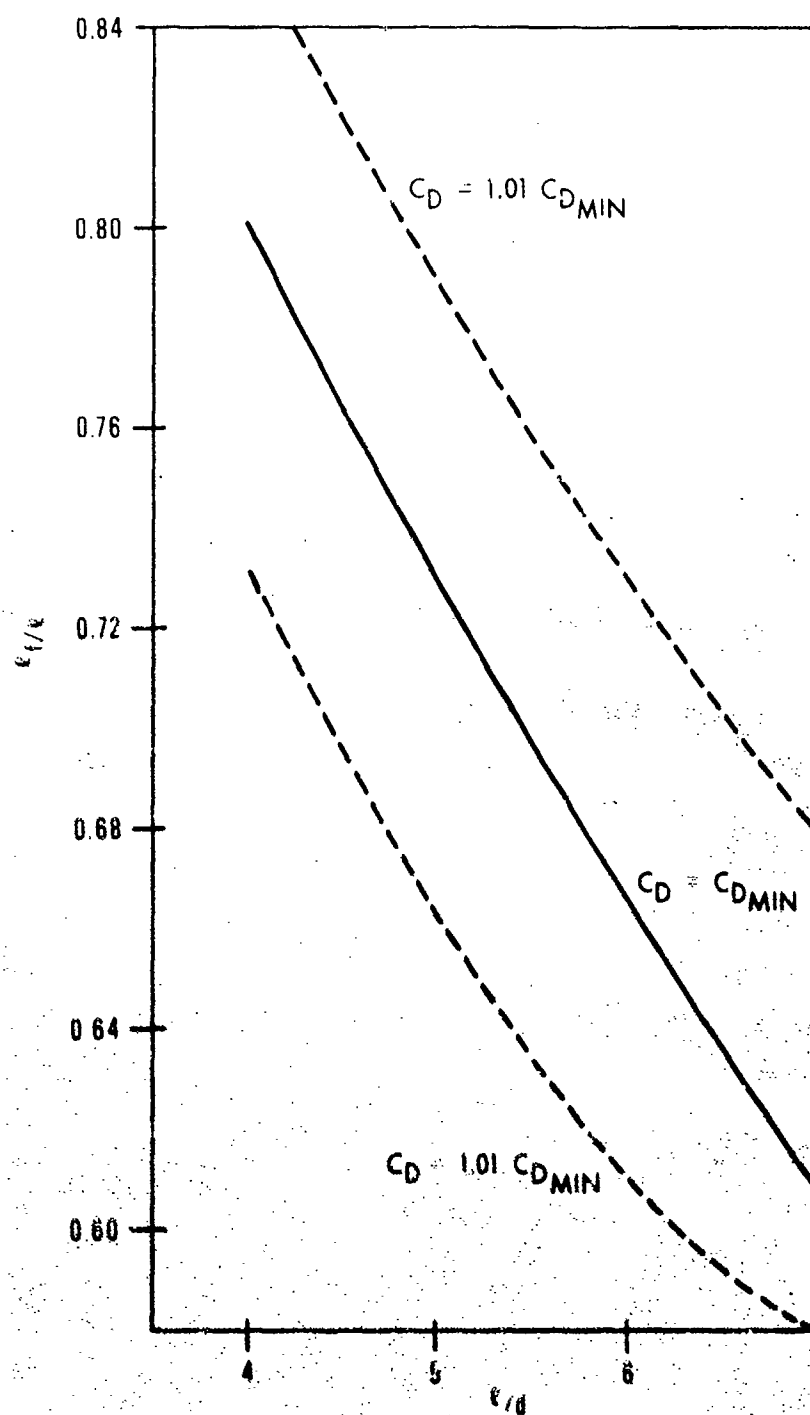


Figure 11 Drag Penalty for Nonoptimum Configurations for $M_\infty = 3$

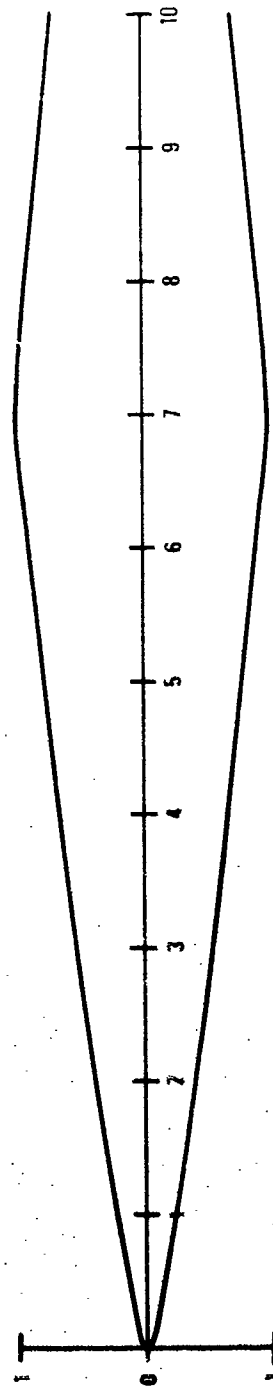


Figure 12. Optimum Body Profile for $M_\infty = 3$, $\eta/H = 5$ Using Approximate Theory

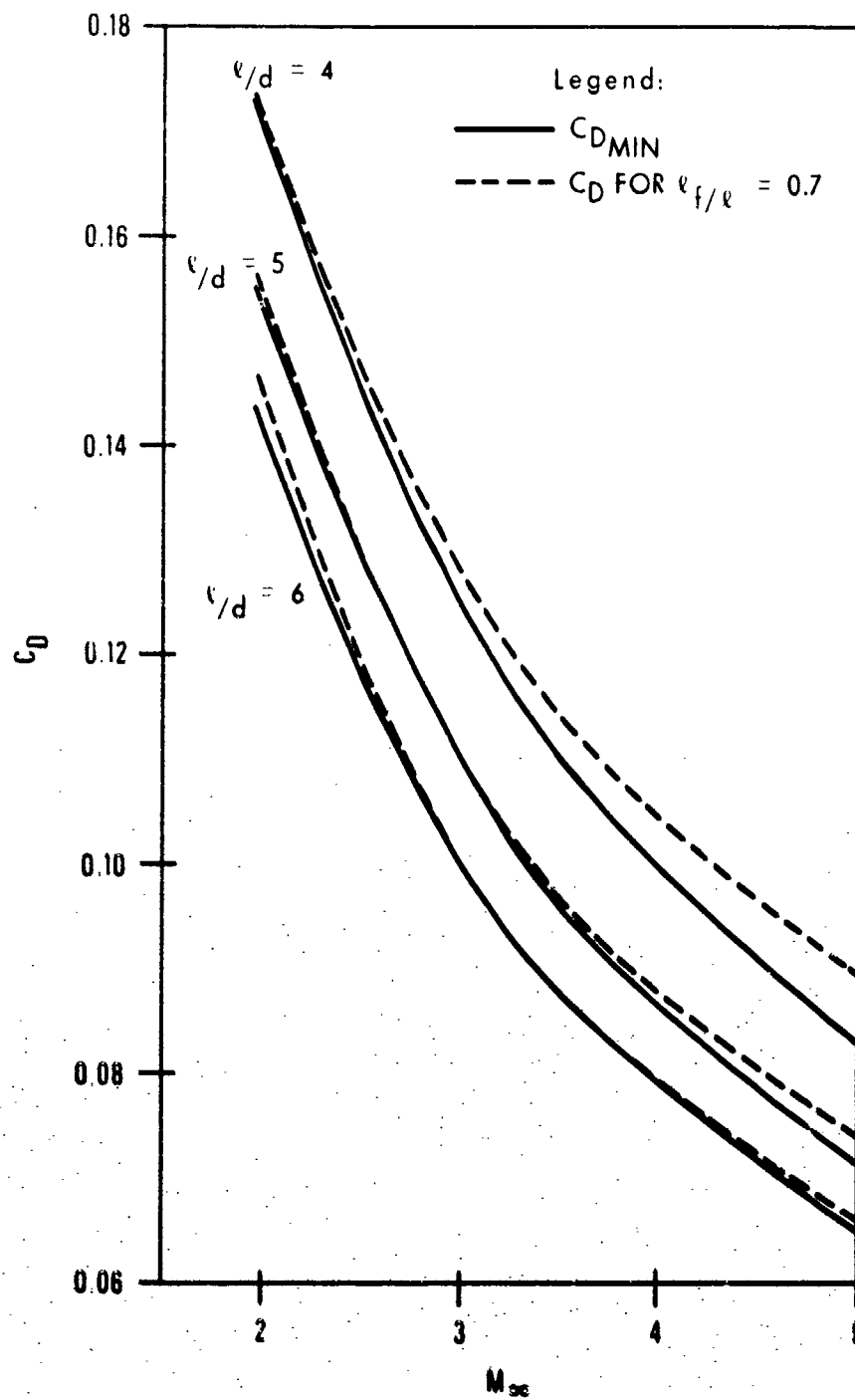


Figure 13 Drag Penalty for Having $l_f/l = 0.7$ as Function of Mach Number

REFERENCES

1. F. G. Moore, *A Study to Optimize the Aeroballistic Design of Naval Projectiles*, Naval Weapons Laboratory Technical Report, NWL TR-2337 Dahlgren, VA, September, 1969.
2. T. Von Karman and N. B. Moore, *Resistance of Slender Bodies Moving with Supersonic Velocities, with Special Reference to Projectiles*, APM-54-27.
3. W. R. Sears, "On Projectiles of Minimum Wave Drag," JAS, Vol. 4, 1947.
4. W. Haack; *Projectile Forms of Minimum Wave Resistance*, Douglas Aircraft Co., Inc. Report No. 288, 1946.
5. C. Ferrari, *The Determination of the Projectile of Minimum Wave Resistance*, Issued as British M.A.P., RTP Technical Report 1180.
6. J. D. Cole, *Newtonian Flow Theory for Slender Bodies*, U.S. Air Force, Project RAND, RM 1633, 1959.
7. T. Strand, "Design of Missile Bodies for Minimum Drag at Very High Speeds. Thickness Ratio, Lift and Center of Pressure Given," JAS, No. 9, pp. 568-570, 1959.
8. A. Miele, *Theory of Optimum Aerodynamic Shapes*, the Academic Press: New York, 1965.
9. A. J. Eggers, M. M. Resnikoff, and D. H. Dennis, *Bodies of Revolution Having Minimum Drag at High Supersonic Airspeeds*, NACA Report 1306, 1958.
10. S. L. Brown, *Axisymmetric Bodies of Minimum Drag*, Dissertation, The University of Texas, Austin, Texas, 1967.
11. L. S. Stivers, Jr. and B. Spencer, Jr., *Studies of Optimum Body Shapes at Hypersonic Speeds*, NASA TN D-4191, 1967.
12. F. G. Moore, *Body Alone Aerodynamics of Guided and Unguided Projectiles at Subsonic, Transonic, and Supersonic Mach Numbers*, Naval Weapons Laboratory Technical Report NWL TR-2796, Dahlgren, VA, November, 1972.
13. J. M. Solomon, M. Ciment, R. E. Ferguson and J. A. Bell, *A Program for Computing Steady Three-Dimensional Supersonic Flow on Reentry Vehicles*, Vol. I Analysis and Programming, Vol. II - User's Manual, NSWC, NOL, (February, 1970 preliminary version).

14. E. R. Van Driest, "Turbulent Boundary Layer in Compressible Fluids," JAS, Vol. 18, No. 3, 1951, pp. 145-160, 216.
15. W. W. Hager, "Rates of convergence for discrete approximations to unconstrained control problems," SIAM J. Numer. Anal., 13 (1976), p. 449-472.
16. W. W. Hager and S. K. Mitler, "Lagrange duality theory for convex control problems," SIAM J. Control, 14 (1976), p. 843-856.

APPENDIX A

GLOSSARY

w_1, w_2	functions defined by Equation (23)
x	distance along body axis of symmetry
z	parameter used in Equation (20)
z_0	critical value of z given by Equation (21)
α	positive root of Equation (22)
γ	ratio of specific heats (1.4 for air)
θ	angle along body surface $\theta = \tan^{-1}(dr/dx)$
λ	dual multiplier
μ	coefficient of absolute viscosity
ρ	air density also $\rho = r^2$ in forebody optimization problem

GLOSSARY

A	} constants defined after Equation (6)
B	
C_1	
C_2	
C_D	drag coefficient
C_{DAB}	afterbody drag coefficient
C_{DF}	forebody drag coefficient
C_{f_w}	mean skin friction coefficient
C_{pB}	pressure coefficient, $C_p = (p - p_\infty) / \frac{1}{2} \rho_\infty V_\infty^2$
C_{pBA}	base pressure coefficient
C_{pBA}	base pressure coefficient on a configuration with a cylindrical afterbody and turbulent flow at the base
C_{p0}	stagnation pressure coefficient
d_B	base diameter
d_r	reference diameter (maximum cross section of body)
g	$1/r'$
g^*	optimal solution
G	value of g which minimizes $III(g, z)$
h	function defined by Equation (19)
H	function defined by Equation (20), also a different function by Equation (34)
ℓ	length of configuration
ℓ_f	forebody length
M	local Mach number
M_∞	freestream Mach number
n	variable defined by Equation (7)
p	pressure
p_0	stagnation pressure
Pr	Prandtl number
p_∞	freestream pressure
R	maximum radius of body $= d_r/2$
R_N	freestream Reynolds number
R_T	turbulent recovery factor
r	radius along body
r_n	blunted nose radius at tip of forebody
r'	body slope, d_r/dx
S_r	reference area $= \pi d_r^2/4$
S_w	wetted surface area of body
T_w	wall temperature
T_∞	freestream temperature
V_∞	freestream velocity

DISTRIBUTION

Commander, Naval Sea Systems Command
Washington, DC 20362
Attn: Mr. Lionel Pasiuk (SEA-03)
Technical Library

Commander, Naval Material Command
Washington, DC 20360
Attn: Mr. Sid Jacobsen (MAT-032)
Dr. John Huth
Technical Library

Commander, Naval Air Systems Command
Washington, DC 20360
Attn: Mr. Bill Volz (AIR-320)
Dr. H. Muller
Technical Library

Commander, Naval Weapons Center
China Lake, CA 93555
Attn: Mr. Ray Van Aken
Mr. D. Meeker
Technical Library

Commanding Officer, Naval Missile Center
Point Mugu, CA 93041
Attn: Mr. Joe Rom
Technical Library

Commander Naval Ship Research and Development Center
Washington, DC 20007
Attn: Dr. T.C. Tai
Technical Library

Commander
Naval Weapons Center
Corona Laboratories
Corona, CA 91720
Attn: Technical Library

Office of Naval Research
Pentagon
Washington, DC 20350
Attn: Dr. R.J. Lundegard
Mr. Dave Seigel
Dr. Bob Whitehead
Mr. Mort Cooper
Mr. Ralph Cooper
Technical Library

(2)

Commanding Officer and Director
Naval Ship Research and Development Center
Carderock, MD
Attn: Technical Library

(2)

Deputy Chief of Naval Operations
(Development)
The Pentagon
Washington, DC 20350
Attn: Technical Library

(2)

Commanding Officer
Naval Air Development Center
Warminster, PA 18974
Attn: Technical Library

(2)

Commanding Officer
Naval Air Development Center
Aeronautical Structures Department
Philadelphia, PA 19112
Attn: Technical Library

(2)

Chief of Naval Research
Department of the Navy
Washington, DC 20360
Attn: Technical Library

(2)

Commander
Pacific Missile Range
U.S. Naval Missile Center
Point Mugu, CA 93041
Attn: Technical Library

(2)

Library of Congress
Washington, DC 20540
Attn: Gift and Exchange Division

(4)

Nielsen Engineering and Research, Inc.
510 Clyde Avenue
Mountain View, CA 94043

Defense Printing Service
Washington Navy Yard
Washington, DC 20374

Commandant of the Marine Corps
Headquarters, Marine Corps
Washington, DC 20380

Attn: Code AX (2)
Code A04F (2)
Code A03H
Technical Library (2)

Local:

DC
DC-40
DC-44
DK
DK-20
DK-21 (Moore) (10)
DK-50
DX-21 (2)
DX-22 (6)
DX-40
DX-43 (Thompson)
WA
WA-40
WA-40 (Regan)
WA-40 (Hastings)
WA-40 (Piper)
WA-40 (Goeller)
WA-40 (Sheetz)
WA-50
WR

North Carolina State University
Department of Mechanical and Aerospace Engineering
Box 5246
Raleigh, NC 27607
Attn: Prof. F.R. DeJarnette
Technical Library

(10)
(2)

The University of Tennessee Space Institute
Tullahoma, TN
Attn: Dr. J.M. Wu
Technical Library

(2)

Defense Documentation Center
Cameron Station
Alexandria, VA 21314

(12)

Director Defense Research and Engineering
Department of Defense
Washington, DC 20301
Attn: Bartley Osborne, R&AT Office

Dr. Jim Zerikos
McDonnell Douglas Astronautics Company (West)
5301 Bolsa Avenue
Huntington Beach, CA 92647
Mail Station 13-2

Dr. Lars E. Ericson
Lockheed Missiles and Space Company, Inc.
Department 81-10, Bldg. 154
Sunnyvale, CA 94088

Mr. B. H. Shirley
Lockheed Missiles and Space Company, Inc.
P.O. Box 1103, W. Street
Huntsville, AL 35807

Mr. V.L. Pianta
Senior Project Engineer
P.O. Box 1201
San Jose, CA 95108

NASA Goddard Space Center
Greenbelt, MD 20771
Attn: Technical Library

(2)

NASA Lewis Research Center
Cleveland, OH 44101
Attn: Technical Library

(2)

NASA
Washington, DC 20546
Attn: Technical Library

(2)

NASA Ames Research Center
Moffett Field, CA
Attn: Mr. Vic Peterson
Mr. John Rakich
Technical Library

(2)

NASA Langley Research Center
Langley Station
Hampton, VA
Attn: Mr. Bud Bobbitt
Mr. Jerry South
Mr. Leroy Spearman
Mr. C.M. Jackson, Jr.
Mr. W.C. Sawyer
Technical Library

(2)

Virginia Polytechnic Institute and State University
Department of Aerospace Engineering
Blacksburg, VA
Attn: Prof. J.A. Schetz
Technical Library

(2)

Stanford Research Institute
Menlo Park, CA 94025
Attn: Dr. Milton Van Dyke
Technical Library

(2)

Raytheon Company
Spencer Laboratory
Burlington, MA 01803
Attn: Steve Pearlswig (Box SL 7167)

AFATL (ADLRA), (DLGC)
Eglin Air Force Base, FL 32542
Attn: Dr. D. Daniel
Mr. C. Butler
Mr. K. Cobb
Mr. E. Sears
Technical Library

(2)

USAF Academy
Colorado Springs, CO 80912
Attn: Technical Library

(2)

Wright Air Development Center
Wright-Patterson AF Base, OH 45433
Attn: Mr. Gene Fleeman (FGC)
Technical Library

(2)

Applied Physics Laboratory
The John Hopkins University
8621 Georgia Avenue
Silver Spring, MD 20910
Attn: Dr. L.L. Cronvich
Mr. Freeman K. Hill
Mr. Edward T. Marley
Dr. Gordon Dugger
Technical Library

(2)

Advanced Research Projects Agency
Department of Defense
Washington, DC 20305
Attn: Technical Library

(2)

Director, Defense Research and Engineering
Department of Defense
Washington, DC 20305
Attn: Technical Library

(2)

George C. Marshall Flight Center
Huntsville, AL 35804
Attn: Technical Library

(2)

Aeronautical Research Laboratory
Wright-Patterson AF Base
Dayton, OH 45433
Attn: Technical Library

(2)

Aeronautical System Division
USAF
Wright-Patterson AF Base
Dayton, OH 45433
Attn: Technical Library

(2)

AF Office of Scientific Research
Washington, DC 20330
Attn: Technical Library

(2)

Arnold Engineering Development Center
USAF
Tullahoma, TN 37389
Attn: Mr. J. Usselson
Mr. W.B. Baker, Jr.
Technical Library

(2)

Headquarters, USAF
Systems Command
Andrews AF Base, MD 20331
Attn: Technical Library

(2)

Headquarters, USAF
Washington, DC 20330
Attn: Technical Library

(2)

Flight Research Center
Edwards AF Base, CA 93523
Attn: Technical Library

(2)

Department of the Air Force
Air Force Rocket Propulsion Laboratory (AFSC)
Edwards, CA 93523
Attn: Major Washburn

U.S. Air Force Systems Command Regional Offices
c/o Department of the Navy
Washington, DC 20360
Attn: Technical Library

(2)

Commanding General, U.S. Army Missile Command
Redstone Arsenal, AL 35809
Attn: Mr. Ray Deep (DRSMI)
Dr. D.J. Spring (DRSMI)
Technical Library

(2)

Commanding General
U.S. Army Material Command AMCRD-TP
Washington, DC 20315
Attn: Mr. Joseph M. Hughes
Technical Library

(2)

Office of Chief of Research and Development
Washington, DC 20310
Attn: Major R. A. Burns
Technical Library

(2)

Commanding Officer
Army Chemical Center
Edgewood, MD 21040
Attn: Technical Library

(2)

Commanding General
Frankford Arsenal
Philadelphia, PA 19104
Attn: Mr. W. Gadomski
Technical Library

(2)

Commanding Officer
Harry Diamond Laboratories
Washington, DC 20013
Attn: Mr. R. Warren
Technical Library

(2)

Commanding Officer of U.S. Army Combat Development Command
Field Artillery Agency
Fort Sill, OK 73503
Attn: Technical Library

(2)

President of U.S. Army Field Artillery Board
Fort Sill, OK 73503
Attn: Technical Library

(2)

Director, Development Center
Marine Corps Development and Education Command
Quantico, VA 22134

Chief of S and R Division
Development Center
Marine Corps Development and Education Command
Quantico, VA 22134

Chief of Air Operations Division
Development Center
Marine Corps Development and Education Command
Quantico, VA 22134

Chief of Ground Operations Division
Development Center
Marine Corps Development and Education Command
Quantico, VA 22134

Marine Corps Liaison Officer
Field Artillery Board
Fort Sill OK 73503
Attn: Technical Library

(2)

Commanding General, Ballistic Research Laboratory
Aberdeen Proving Ground, MD 21005
Attn: Dr. C.H. Murphy
Mr. L. McAllister
Mr. A. Platon
Mr. B. McCoy
Technical Library

(2)

Commanding General, Picatinny Arsenal
Dover, NJ
Attn: Mr. A. Loeb
Mr. Mertz
M. Cline
Technical Library

(2)

Director
Naval Strategic Systems Projects Office (PM-1)
Department of the Navy
Washington, DC 20360
Attn: Technical Library

(2)

Superintendent
U.S. Naval Academy
Annapolis, MD 21402
Attn: Head, Weapons Department
Head, Science Department
Technical Library

(2)

Superintendent
U.S. Naval Postgraduate School
Monterey, CA 95076
Attn: Head, Mechanical Engineering Dept.
Head, Department of Aeronautics
Technical Library

(2)

Officer in Charge
U.S. Naval Scientific and Technical Intelligence Center
U.S. Naval Observatory
Washington, DC 20360
Attn: Technical Library

(2)

Commander
Naval Undersea Warfare Center
3203 East Foothill Blvd.
Pasadena, CA 91107
Attn: Technical Library

(2)

Commanding Officer
Naval Ordnance Station
Indian Head, MD 20640
Attn: Technical Library

(2)